J. Electrochem. Sci. Eng. **12(3)** (2022) 545-556; http://dx.doi.org/10.5599/jese.1314

Open Access : : ISSN 1847-9286
https://pub.iapchem.org/ojs/index.php/JESE

Original scientific paper

Palmyra palm flower biomass-derived activated porous carbon and its application as a supercapacitor electrode

Sofia Jeniffer Rajasekaran and Vimala Raghavan✉

Centre for Nanotechnology Research, Vellore Institute of Technology, Vellore, Tamil Nadu, India

Corresponding author: ✉lvimala.r@vit.ac.in

Received: February 26, 2022; Accepted: May 20, 2022; Published: May 25, 2022

Abstract

Due to its abundant availability, eco-friendliness, and high sustainability, biomass-derived activated carbon has captured more attention in recent years. In this study, activated carbon was derived from Palmyra palm flowers (PPF) using a conventional chemical activation process and carbonization at different ambient temperatures, viz. 700, 800, and 900 °C. The carbonized PPF was chemically activated using 1 wt.% potassium hydroxide to increase the microporosity and specific surface. The experimental data were analyzed using X-ray diffractometer (XRD), scanning electron microscopy (SEM), energy-dispersive X-ray spectrometer (EDX), Raman spectroscopy and Fourier transform infrared spectroscopy (FT-IR). The nitrogen adsorption/desorption isotherm curve for activated carbon synthesized at the activation temperature of 900 °C indicated type IV with a hysteresis loop associated with mesopores formation and a specific surface area of 950 m^2g^{-1}. The supercapacitor electrodes made with PPF-derived carbon were evaluated for their electrochemical performance by electrochemical impedance spectroscopy, cyclic voltammetry, and galvanostatic charge/discharge measurements. In the aqueous electrolyte (3 M KOH), electrochemical experiments showed that PPF-900 electrode has a specific capacitance of 155 F g^{-1} at 1 A g^{-1} and significant cyclic stability (97.3 % capacitance retention over 5000 cycles at 10 A g^{-1}), while energy and power densities were estimated as 15.1 Wh kg^{-1} and 100.6 W kg^{-1}. This study suggests that biowaste products could be transformed into activated carbon materials to improve the performance of energy storage materials, and it adheres to the 'waste to treasure' principle.

Keywords

Biowaste products; chemical activation; potassium hydroxide; electrochemical measurements; specific capacitance; energy storage

Introduction

There has been an urgent need in recent years for energy storage devices with quick charging/discharging, high energy density, and long-term cyclability [1]. Based on their charge storage mechanisms, electrochemical capacitors are categorized into two types, *viz*. electrochemical double-layer capacitors (EDLCs) and pseudocapacitors. The EDLC has distinct advantages such as rapid charging time, operational safety, pulse power supply, and outstanding service life [2]. It stores the charge electrostatically at the electro-active material surface *via* reversible ion adsorption and desorption (a

non-faradaic process). In comparison, the primary charge storage mechanism in pseudocapacitors is a quick and reversible redox reaction (faradaic process). Owing to its excellent cycle stability, greater power capability, inexpensive, simple manufacture, and nontoxicity, the main commercially available supercapacitors, *i.e.,* EDLCs, utilize several carbon-based materials as active electrode materials [3]. Supercapacitors are the substitutional power sources for conventional batteries for applications including energy harvesting systems, electrical vehicles, and portable electronic devices. Hence, there is increasing attention towards research in new electrode materials with high performance, high stability, cost-effectiveness, and eco-friendliness. Activated carbon with abundant pore structures is researched extensively for energy storage devices, particularly supercapacitors, over the last ten years [4]. Researchers have begun to focus on newly activated carbon precursors, which are of relatively low cost, chemically stable, highly electrically conductive, of high specific surface area, and well-built hierarchical pore structure [5]. Because of their renewable nature, accessibility, and availability, biomass wastes are currently being employed as precursors for the preparation of activated carbon. Agro-industrial by-products and residues can be transformed into activated carbon. Being a precursor for producing activated carbon, almost any carbon-containing material can be utilized [6]. Several studies have considered the possibility of synthesizing activated carbon from biowaste products like chestnut shell [7], *Xanthoceras sorbifolia* seed coats [8], tea seed shell [9], pine sawdust [10], dead neem leaves [11], rice husk [12,13], pomelo peels [14], *etc*. In general, physical and chemical activation procedures can convert these raw materials to activated carbon. The use of activation gas, such as CO_2, steam, or a combination of gases, is followed to prepare the activated carbon by a physical activation process. During the process of chemical activation, the carbon precursor is combined with chemicals like KOH, NaOH, H_3PO_4, H_2SO_4 and $ZnCl_2$. KOH was reported as the most effective agent for activation, able to suppress tar formation, reduce the temperature of the activating reaction, and expedite the exclusion of non-carbon components, apart from boosting the pyrolysis efficiency [15].

KOH-treated activated carbons are prepared by combusting activated carbon precursors in an oxygen-free environment. They have wider pore sizes and volumes and higher specific surface area than activated carbon precursors that have not been KOH treated. The activated carbon precursor and the carbon products acquired by potassium hydroxide chemical activation may differ significantly in surface topography compared to physical activation approaches such as CO_2 and steam. The specific surface area and characteristic pore structure of carbon materials are essential for electrochemical energy storage applications. To improve the capacitive ability, surface functional groups combining nitrogen, oxygen, and sulphur can produce pseudocapacitive behavior and promote wettability. As a result, new and low-cost, environmentally sustainable biowaste products with the role of facilitating economic development for energy and environmental domains have attracted a great deal of attention. Liu *et al*. [16] used KOH-based chemical activation to create activated carbon from soybean pod biomass as electrode materials for supercapacitors. The carbon exhibited good electrochemical properties, with a specific capacitance of 321 F g^{-1} at 1 A g^{-1} current density attributed to the high specific surface area (2245 m^2 g^{-1}), distribution of pore sizes, and structural features rich in oxygen and nitrogen [16]. Taking this into consideration, this work is focused on the investigation of the Palmyra palm flowers (PPF) based activated carbon. Palmyra palm (*Borassus flabellifer* L.) is a well-known member of the Arecaceae family with its origin from India, the Philippines, Laos, Bangladesh, Malaysia, Thailand, Cambodia, Burma, Sri Lanka, Vietnam, and Indonesia. It is discarded as a waste material that gets degraded without being used effectively. Because of its low cost and abundant availability, it could be a feasible biological renewable resource and a promising carbon precursor for obtaining activated carbon.

Experimental

Materials and chemicals

The Palmyra palm flowers were collected on a local agricultural farm in Vellore district, Tamil Nadu, India. The collected palm flowers, which were dry, dark brown and of stick-like elongated structures, were cut into small pieces. These pieces were thoroughly washed with DI water to eliminate dirt particles and dried for 24 hours at 80 °C before being crushed into powder. The powdered samples were stored in a desiccator for further study.

The carbon (graphitized carbon black, 99.95 %) and polyvinylidene fluoride (PVDF), and carbon foil (0.2 mm thick, 99.8 %) were procured from Alfa Aesar. All solvents, including potassium hydroxide (KOH), N-methyl-2-pyrrolidone (NMP), and ethanol (CH_3CH_2OH, 99 %), were procured from Sigma Aldrich. Hydrochloric acid (30 %) was procured from SD Fine-Chem Limited, India. Throughout the experiments, deionized water (DI) was used.

Preparation of porous activated carbon

The powdered Palmyra palm flowers were carbonized for 3 hours at 400 °C. The heating rate was 5 °C min^{-1} under a nitrogen atmosphere before being cooled to ambient temperature. After carbonization, the Palmyra palm flowers were mixed with potassium hydroxide at wt.% of 1:1. To produce activated carbon at three different temperatures, *viz*. 700, 800, and 900 °C, the mixture was subjected to activation in a nitrogen atmosphere for 1 hour at a rate of 5 °C min^{-1}. The obtained activated carbon samples were allowed to reach room temperature and washed with hydrochloric acid solution and distilled water to maintain a neutral pH. Finally, the washed activated carbon samples were kept overnight in a hot oven at 60 °C for drying and designated as PPF-X. Here, X indicates different activation temperatures (700, 800, and 900 °C). The steps followed in the synthesis procedure of Palmyra palm flower-derived activated carbon are depicted in Scheme 1.

Scheme 1. *Schematic of the synthesis of Palmyra palm flower-derived activated carbon*

Characterization

The crystallinity of porous activated carbon was investigated using powder X-ray diffraction (Bruker D8 ADVANCE diffractometer, Germany) with Cu Ka (15.406 nm) radiation. Raman spectra

were analyzed using a HORIBA Jobin Yvon LabRAM ARAMIS excited at 633 nm. The morphology and elements of the sample were evaluated using SEM and energy dispersive X-ray analysis (EDX), ZEISS Neon 40 SEM microscope. The surface functional groups of the synthesized PPF-derived activated carbon were characterized using a Fourier Transform Infrared (FT-IR) spectrometer (Bruker, TENSOR 27 spectrometer). N_2 adsorption/desorption isotherms were measured (Beishide 3H-2000PS2) to determine the surface area, pore size, and pore volume of the prepared activated carbon samples.

Electrochemical measurements

Electrochemical analyses were carried out on a CHI 660C electrochemical workstation, with cyclic voltammetry, charge-discharge, and electrochemical impedance spectroscopy performed in 3M KOH aqueous solution as the electrolyte. Platinum foil and Ag/AgCl (saturated KCl) served as the counter and reference electrodes in the three-electrode system. The active materials (85 %), polyvinylidene fluoride (5 %), and carbon black (10 %) were mixed in N-methyl-2-pyrrolidone solvent (few drops) to get the active electrode ink and further employed as the working electrode. The obtained mixture was coated on a graphite foil substrate (1 cm^2) and subjected to drying in an oven at 80 °C for 12 hours. The coated electrode was used as a supercapacitor electrode and tested with various tests to analyze its efficiency. The active material mass loading for each electrode was approximately 0.002 g. Cyclic voltammetry and galvanostatic charge/discharge (GCD) measurements were carried out at 0 to 0.4 V (potential window) at different scan rates and current densities. The CV measurements were performed in a three-electrode cell system, and the specific capacitance is calculated using the equation (1):

$$C_S = \frac{A}{2mk\Delta V} \tag{1}$$

where C_s is specific capacitance (F g^{-1}), A is the area of CV curve, m is total mass of active material (g), k is scan rate and ΔV is potential window (V).

Equation (2) was used to calculate the specific capacitance of the supercapacitor electrode from charge/discharge curves:

$$C_S = \frac{I\Delta t}{m\Delta V} \tag{2}$$

where I is imposed constant current (A), and t is discharge time (s).

The energy density (E_D) and power density (P_D) values were calculated from galvanostatic charge/discharge measurements according to:

$$E_D = \frac{1}{2}C_S\Delta V^2 \tag{3}$$

$$P_D = \frac{E_D}{\Delta t} \tag{4}$$

Electrochemical impedance spectroscopic analyses of PPF electrodes were recorded at 0.3 V in the frequency range of 100 kHz to 0.1 Hz, with an amplitude of 0.005 V of AC voltage. Impedance (Z) was expressed as the real (Z') and imaginary ($-Z''$) components.

Results and discussion

Figure 1a depicts the X-ray diffraction patterns of the activated carbon prepared at different temperatures. All three activated porous carbon samples didn't show any sharp peaks, indicating that they are weakly crystallized. Less intense peaks at 23 and 42° correspond to graphitic carbon planes (002) and (100), indicating the presence of amorphous carbon. The broad diffraction peak

with low peak intensity centered at 2θ = 23° could be indexed as highly disordered graphite [17]. The reduced intensity of the diffraction peak with KOH activation is attributed to the turbostratic carbon structure in PPF with randomly oriented graphene layers. Raman spectra further confirmed the presence of a graphitic phase as observed in Figure 1b, where the D-band represents the disordered carbon layer structure and defects in the carbon material, whereas G-band represents the vibration of sp^2 hybridized carbon atoms in the graphite sheet structure [18]. It denotes the carbon phases of diamond (D) and graphite (G) at 1353 and 1597 cm^{-1}, respectively. The term I_D/I_G (the ratio of D band to G band intensity) is commonly used to describe the degree of carbon disorder. The intensity of the G band is slightly greater than the intensity of the D band, indicating that the prepared samples contain more structurally ordered graphite. The higher I_D/I_G value of the PPF-900 indicated that the PPF-900 had more defective (amorphous) carbon structures than other synthesized at the other two temperatures, which was induced by KOH activation.

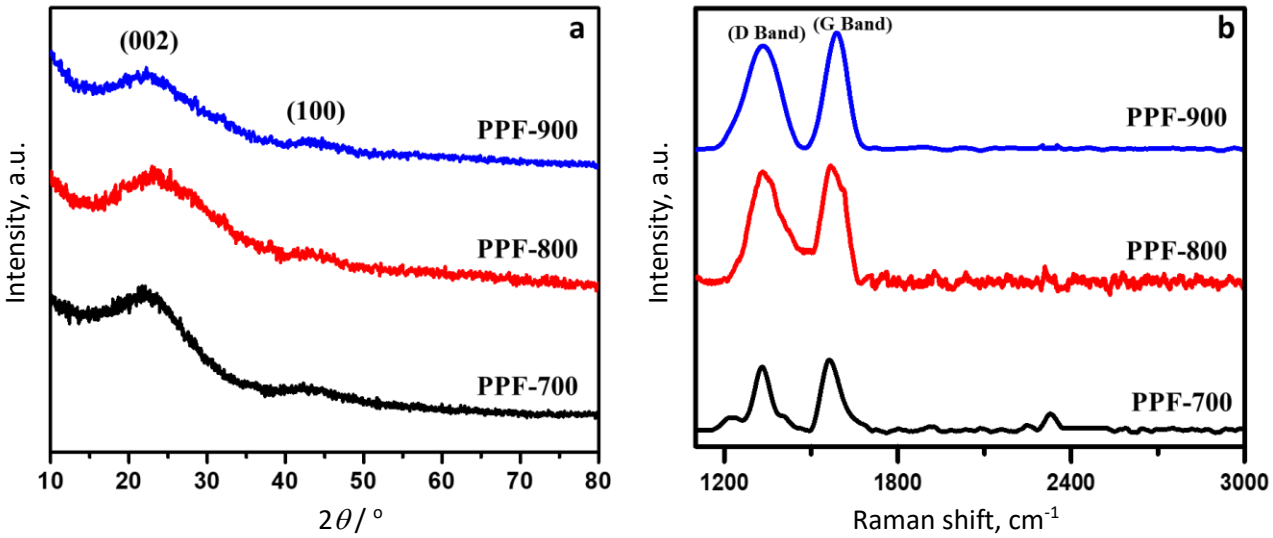

Figure 1. *(a) XRD patterns and (b) Raman spectra of PPF-700, PPF-800, and PPF-900 activated carbon*

The values of I_D/I_G (the intensity ratio of D band to G band) varied with activation temperature, with PPF-900 having the highest I_D/I_G value of 0.89 and PPF-700 and PPF-800 gave I_D/I_G values of 0.86 and 0.82, respectively, indicating that the defect structures in sample PPF-900 are more disordered. As the activation temperature was raised, the I_D/I_G ratio gradually increased, implying that the order of the graphitic structure was destructed and that high-temperature activation increased the presence of defects in PPF-900. Results showed that a significant KOH ratio (1:1) inhibits graphitization and increases the disorder of the material microstructure, which is consistent with the XRD results. To further evaluate the properties of the surface and chemical composition of the carbonized sample, *viz*. PPF-700, PPF-800, and PPF-900, the materials were investigated using FTIR (Figure 2).

All carbon samples prepared from Palmyra palm flowers have functional groups on their surfaces, confirming the presence of oxygen. O–H stretching vibrations were assigned to broadband in the region of 3157 cm^{-1} [19]. The presence of O–H and carboxyl groups has been figured out to improve electrode wettability and electrochemical performance. C=N stretching vibrations are assigned for the peak at 2085 cm^{-1} [20]. C-C vibration in aromatic rings and C-O stretching could be assigned to the 1521 cm^{-1} and 1062 cm^{-1} bands, respectively [21,22]. The presence of surface functional groups in activated carbon derived from PPF could be attributed to potassium hydroxide activation.

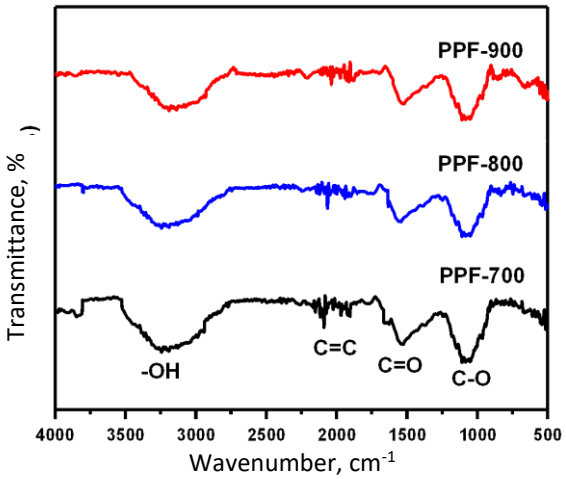

Figure 2. *FTIR spectra of PPF-700, PPF-800, and PPF-900-activated carbon*

Figure 3(a-c) shows SEM images of activated porous carbon samples synthesized at three temperatures and the respective EDAX. After carbonization, all samples exhibited a significant porous structure, which is necessary for active ion transport and higher surface area, and thereby the efficient storage of charge. The surfaces of PPF-700, PPF-800, and PPF-900 confirm the formation of disordered carbon structure due to the release of volatile compounds during the carbonization procedure.

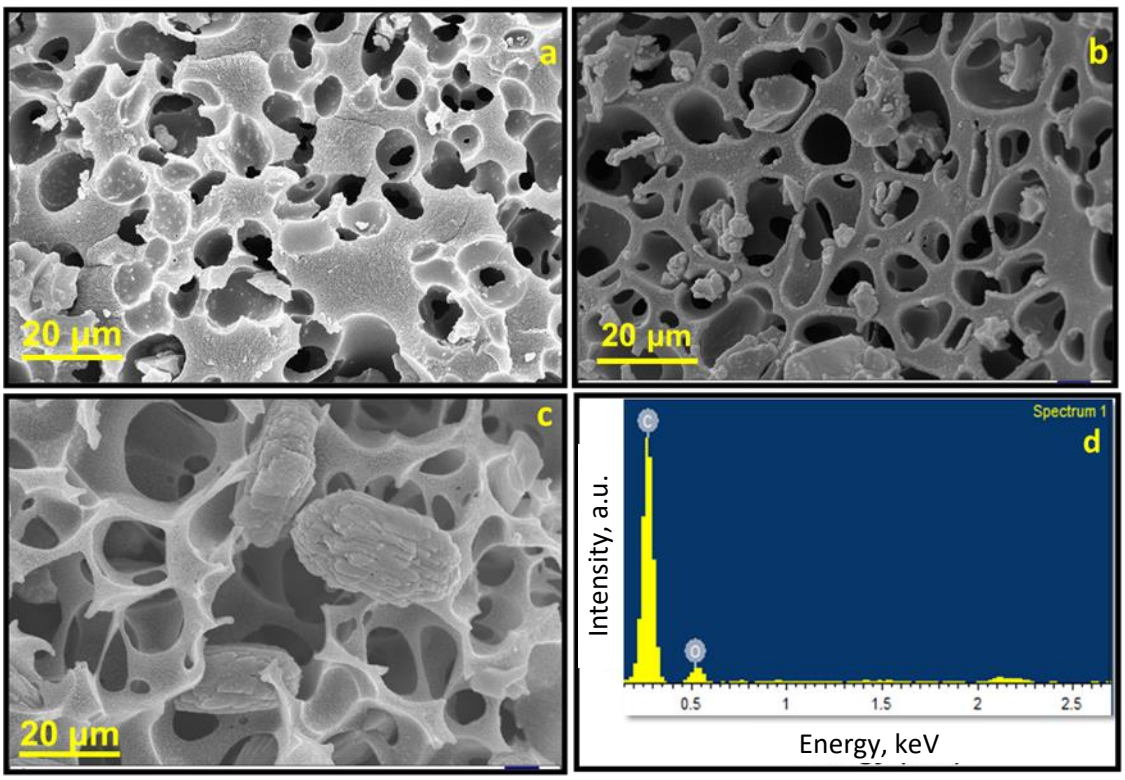

Figure 3. *(a-c) SEM images of PPF-700, PPF-800, and PPF-900 based activated carbon at magnification 20,000 ×; (d) EDAX analysis of PPF-900*

The chemical treatment created large pores, which aided in the activation of the carbon particle internal surfaces. For supercapacitor electrodes, the porous structure of activated carbon creates an ideal surface environment for ion diffusion during the charge-discharge process [23]. Furthermore, EDAX was used to examine the elements of the Palmyra palm flower-derived activated carbon. The EDAX spectrum of PPF-900 activated carbon presented in Figure 3d shows that it

consists of 88.81 % of carbon weight and 9.65 % of oxygen weight. The high carbon content indicates that most of the PPF-900's got volatilized, and non-carbon content was removed during the activation process, resulting in much higher carbon content.

The nitrogen adsorption/desorption isotherms from BET isotherms are given in Figure 4a. The Palmyra palm flower-derived carbon isotherm at PPF-900 is classified as type IV because it is horizontal and parallel throughout the (p/p_0) range. The internal surface area is represented by the BET surface area, which is generally in two forms, such as micropores and mesopores. The micropores surface area identifies the percentage of microporous activated carbon [24]. The PPF-900 gave a surface area of 950 $m^2\ g^{-1}$ as a result of different types of pores formed during chemical activation. The steep growth at low pressure and narrow hysteresis loop indicates the presence of micropores. An increased activation temperature has increased specific surface area and pore volume. As an activator, KOH significantly affects pore development [25]. Increasing the carbonization temperature to 900 °C causes the precursor to release more volatile compounds, resulting in an increased pore development and the formation of new pores. Further, as observed from the pore size distribution curve (Figure 4b), the average pore size was calculated to be 1.7 nm, revealing that the obtained activated carbon exhibits a microporous structure.

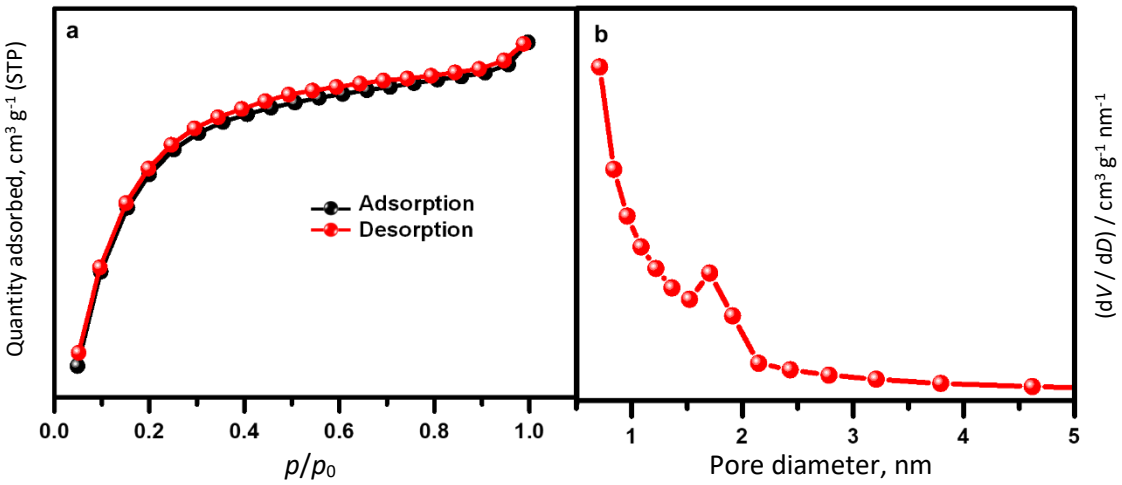

Figure 4. *(a) N_2 adsorption-desorption isotherms (STP - standard temperature and pressure); (b) pore size distribution of PPF-900*

The porous structures were obtained through the chemical etching reactions during the KOH activation process and as a result, micropores are the most potential sites where charges are held at electrolyte/electrode double-layer interfaces. In brief, the specific surface area of PPF-900 and hierarchical micropore distribution can promote electrolyte ion penetration and diffusion and provide significant surface area that is electrochemically active for double-layer charging/discharging.

Electrochemical investigations

The CV and GCD curves of PPF-700, PPF-800, and PPF-900 samples were evaluated in a three-electrode system using 3 M KOH as the electrolyte, in order to analyze the influence of activation temperature on the electrochemical performance of the electrode material derived from Palmyra palm flowers. All CV curves in the voltage range of 0 - 0.4 V have an approximately quasi-rectangular voltammogram shape, as given in Figure 5a, indicating good charge propagation without significant redox peaks. The rate of ion transport/diffusion in carbon material can be determined by the shape of the CV curve [26]. Among three PPF electrodes activated at different temperatures, the PPF-900 electrode has the largest area as observed from the CV curve, indicating higher specific capacitance

than for other electrodes. Specific capacitance values calculated using Eq. (1) for PPF-700, PPF-800, and PPF-900 electrodes were 13, 29 and 76 F g^{-1}, respectively. The shape of the CV curves changes as the activation temperature rises, resulting in an enhancement in the CV curve area and current density. Despite a high scan rate (100 mV s^{-1}), the PPF-900 maintained symmetric and rectangular CV curves. This could be due to the electrode material surface area, large microporosity, and low internal resistance. PPF-900 has the largest integrated area and the longest charge-discharge time, indicating the highest specific capacitance. Figure 5b depicts the GCD curves of electrodes with active material formed at various temperatures, measured at a current density of 1 A g^{-1}. The curves are linear and unsymmetrical, confirming that PPF-700, PPF-800, and PPF-900 electrodes are almost reversible. The slope of the electrode discharge curve decreased slightly as the activation temperature increased, indicating an increase in specific capacitance. Figure 5c shows specific capacitance for PPF-700, PPF-800, and PPF-900, calculated from the GCD curves using Eq. (2). It is clear that PPF-900 exhibited higher specific capacitance than PPF-700 and PPF-800 at all current density values applied (1-10 A g^{-1}). At a current density of 1 A g^{-1}, the specific capacitances of PPF-700, PPF-800, and PPF-900 are 100, 138 and 155 F g^{-1}, respectively. The specific capacitance values obtained by GCD were higher than that obtained by CVs, which might be attributed to different current densities (1-10 A g^{-1} in GCD and 0.01-0.02 A g^{-1} in CV) in two different techniques. Supercapacitors are power sources operating at higher currents, and in order to check the performance and stability of prepared electrodes, GCD measurements were performed at higher current densities [27].

EIS results of all three electrodes, developed from activated carbons synthesized at different temperatures, are shown in Figure 5d. At high frequencies, the Nyquist plot is a depressed semicircle, followed by a more or less visible sloping line in the high to the middle-frequency region and a prominent inclined vertical tail at low frequencies [28]. Such a shape of Nyquist plots is characteristic of the impedance response of highly porous capacitive electrodes, where an inclined vertical line at low frequencies is directly attributed to a non-ideal capacitive response of electrode material [29]. The semicircle response at higher frequencies can be associated with surface properties of porous active material, charge transfer of some possible pseudocapacitive reaction (such of surface functionalities), and/or contact impedance generated between active material and current collector. The impedance seen as a linear sloping line at high to medium frequencies is characteristic for diffusion of electrolyte ions within a porous material. Resistive components of all these impedances contribute to the internal electrode resistance value, which is generally determined by the electronic resistance of activated carbon particles, electronic resistance of the current collector to the active material and ionic resistance of electrolyte distributed within the pores. In a Nyquist plot, internal electrode resistance can be roughly defined by two impedance curve intercepts at Z' axis, *i.e.,* of the semicircle at high frequencies and the capacitive line at low frequencies [30,31].

The vertical line represents the non-Faradaic, *i.e.,* purely capacitive impedance of a porous activated carbon electrode, where specific capacitance in F/g can be determined from Z'' value at some low frequency where $Z'' >> Z'$, according to:

$$C_s = (2\pi f Z'' m)^{-1} \quad (5)$$

In Eq. (5), Z'' is the imaginary part of impedance (Ω) measured at the frequency f (Hz), and m is the mass of active electrode material (g). From EIS, the specific capacitance calculated for PPF-700, PPF-800, and PPF-900 at f = 0.1 Hz, are 6.9, 7.8 and 10 F g^{-1}, respectively. Due to the steady-state in EIS measurements, the values of C_s are rather small. Although at f= 0.1 Hz, the condition $Z'' >> Z'$ was not strictly fulfilled (Figure 5d), the order of C_s values can be considered reliable. Thus, the

higher specific capacitance of PPF-900 could be attributed to higher porosity and thereby higher surface area and the improved electrolyte transport in the electrodes.

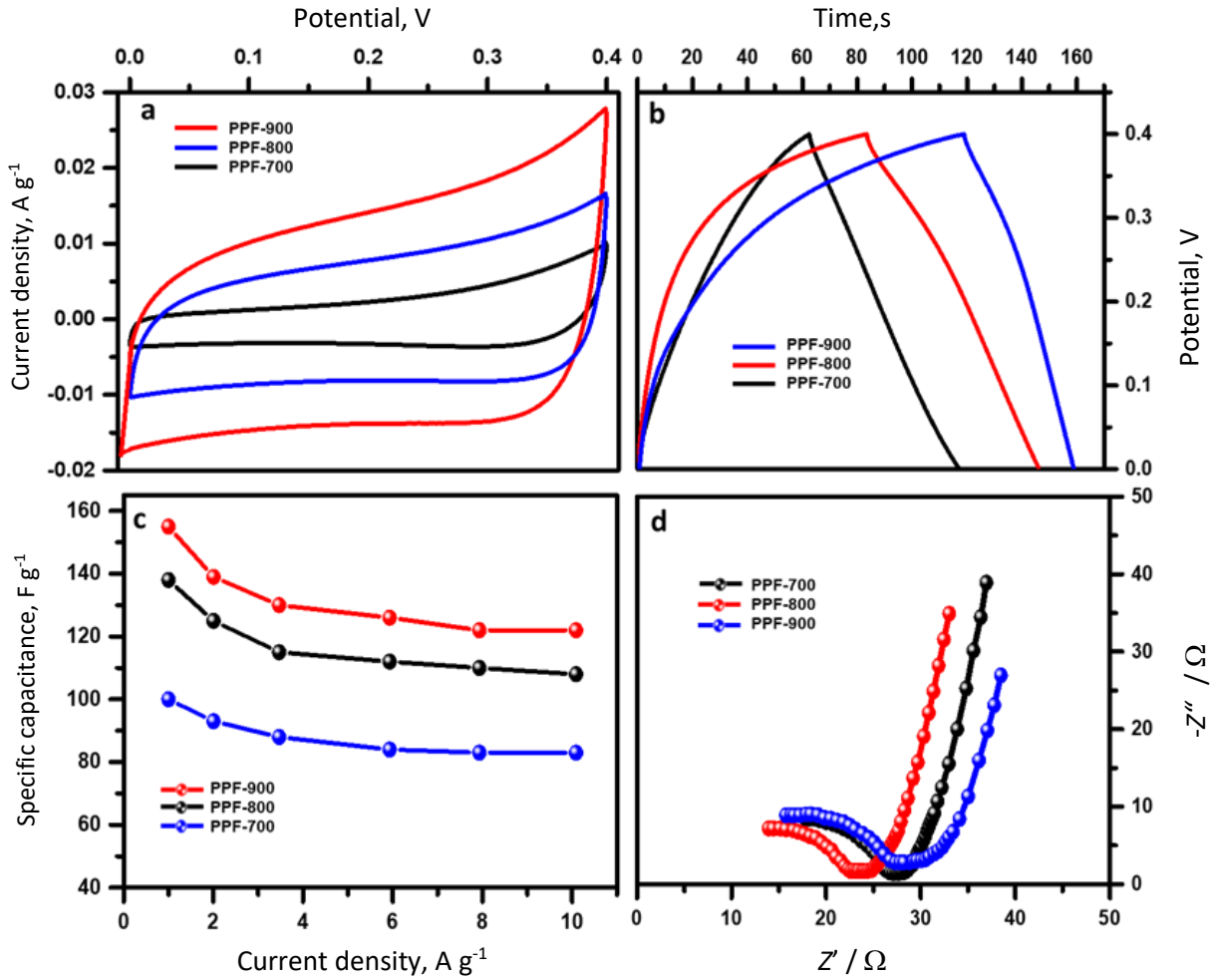

Figure 5. *Electrochemical performance of PPF-700, PPF-800, and PPF-900 activated carbon electrodes: (a) cyclic voltammetry at scan rate of 100 mV s^{-1}; (b) galvanostatic charge-discharge curves at current density of 1 A g^{-1}; (c) specific capacitance at different current densities; (d) Nyquist plots measured at 0.3 V in the frequency range from 100 MHz to 0.1 Hz in 3 M KOH*

Figure 6a shows CV curves of the PPF-900 sample at scan rates ranging from 10 to 100 mV s^{-1}, while Figure 6b shows GCD curves of PPF-900 at various current densities ranging from 1 to 10 A g^{-1}. Furthermore, as current density increases, charge-discharge time decreases significantly because electrolyte ions have much time to enter and diffuse into the porous structures at reduced current densities [32].

A typical double-layer response is characterized by triangular shapes with excellent symmetry. The discharge time of PPF-900 was significantly longer than that of PPF-700 and PPF-800 activated carbon at high current densities, indicating that the PPF-900 has a significantly greater charge-storage ability, which is in accordance with CV experiment results. Due to the high surface area, well-distributed micropores, and thick pore walls in PPF-900, it delivered a capacitance of 120 F g^{-1} at 10 A g^{-1}, indicating good stability in electrochemical studies.

As given in Figure 6c, the Ragone plot calculated from GCD experiments showed that PPF-900 symmetric supercapacitor would have a maximum energy density of 15.1 W h kg^{-1} and retained power density of 100.6 W kg^{-1} in 3 M KOH electrolyte, indicating that the as-prepared electrodes have an excellent rate capability.

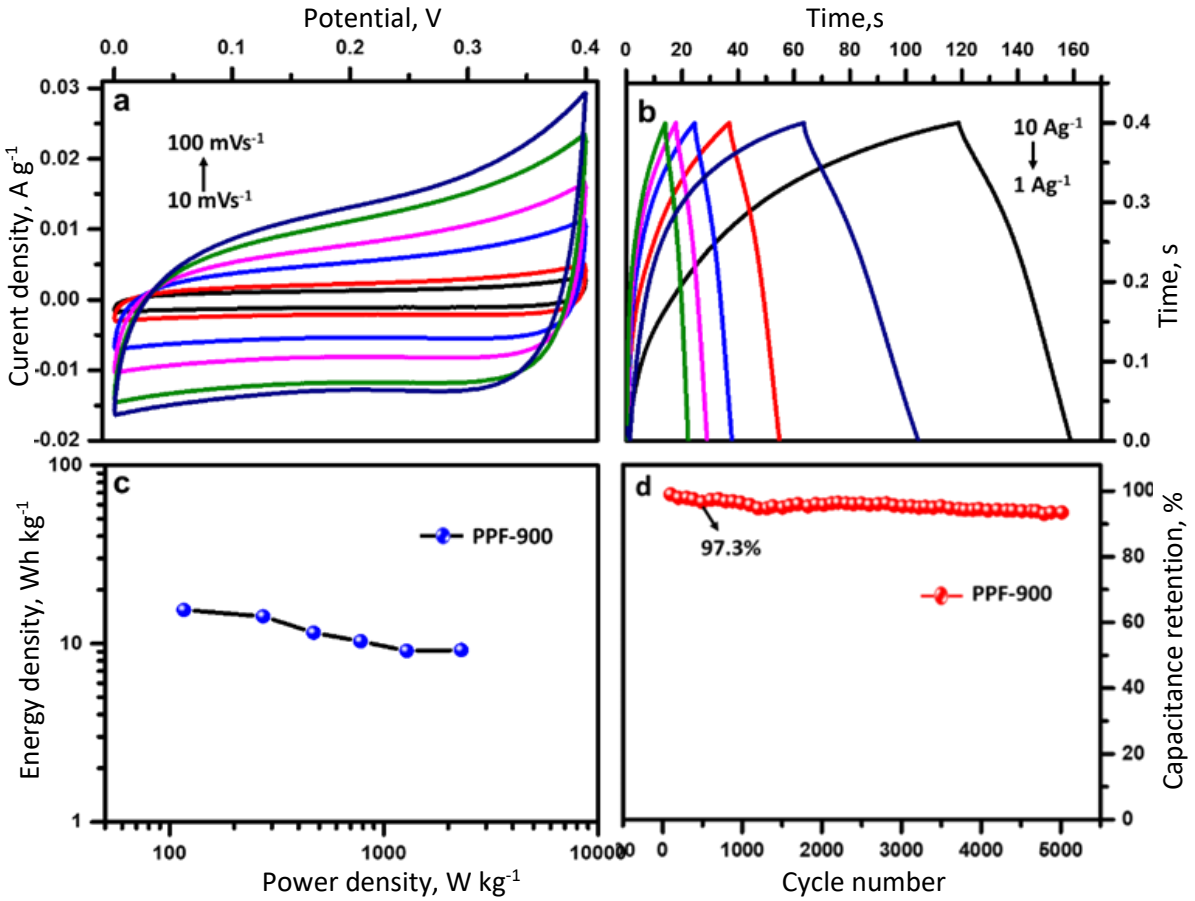

Figure 6. *Electrochemical characteristics of PPF-900: (a) cyclic voltammograms at scan rates from 10 to 100 mV s^{-1}; (b) GCD curves at different current densities (1 to 10 A g^{-1}); (c) Ragone plot of PPF-900; (d) cyclic stability of the electrode at 10 A g^{-1} for 5000 cycles*

The capacitive performance of PPF-900 was considerably higher than that of other activated carbon materials derived from biomass (Table 1).

Table 1. *Comparison of the capacitive performance of supercapacitor electrode of biomass-derived porous activated carbon from different precursors with the reported work*

Biomass	Activating agent	Specific capacitance, F g^{-1}	Current density, A g^{-1}	Electrolyte	Reference
Red cedar	HNO_3	115	0.5	H_2SO_4	[33]
Rotten carrot	$ZnCl_2$	135	0.5	KOH	[34]
Cassava peel waste	KOH	153	10.0	H_2SO_4	[26]
Sago waste	KOH	64	0.1	H_2SO_4	[35]
Banana fiber	$ZnCl_2$	74	0.1	Na_2SO_4	[36]
Coffee shells	$ZnCl_2$	150	0.5	KOH	[37]
Rice husk	KOH	80	0.1	KOH	[12]
Tobacco waste	KOH	148	0.5	KOH	[38]
Waste tire	H_3PO_4	106	1.0	KOH	[39]
Palmyra palm flower	KOH	155	1.0	KOH	This work

The long cycling stability of PPF-900 was tested using GCD at a current density of 10 A g^{-1}, as given in Figure 6d. The capacitance remained at 97.3 % after 5000 cycles despite a slight change in the shapes of the charge and discharge curves. The capacitance value was observed to increase in the first 500 cycles and thereafter decreased, owing to an increase in wettability of the electrode material over a precise number of cycles. These findings confirmed that the electrode based on PPF-900 was highly reversible and stable. Thus, Palmyra palm flower activated at 900 °C exhibited good electrochemical performance, which can be attributed to high specific surface area facilitating the development of

electrochemical double layers and appropriate pore size that facilitates quick ion transport, resulting in an effective improvement in the charge-discharge process.

Conclusions

In this work, porous activated carbon was developed by chemically activating Palmyra palm flowers in KOH and subsequent carbonization at different temperatures for perceiving the effect of temperature on the intrinsic properties of the obtained activated carbon. Palmyra palm flower-derived activated carbon demonstrated good EDLC behavior in 3 M KOH electrolytes, with high specific capacitance and remarkable reversibility. The porous carbons activated at 900 ^{o}C, among other activation temperatures, have a high specific surface area of 950 m^2 g^{-1} with a maximum specific capacitance of 155 F g^{-1} at 1 A g^{-1}. Furthermore, the electrodes have an energy density of 15.1 Wh kg^{-1}, a power density of 100.6 W kg^{-1}, and stable cycle life of over 5000 at 10 A g^{-1}. These results demonstrated the interesting nature of using biomass waste to develop cost-effective electrode materials for supercapacitors with high performance.

References

[1] X. Fan, B. Liu, J. Liu, J. Ding, X. Han, Y. Deng, X. Lv, Y. Xie, B. Chen, *Transactions of Tianjin University* **26(2)** (2020) 92-103. https://doi.org/10.1007/s12209-019-00231-w.

[2] C. Merlet, B. Rotenberg, P.A. Madden, P. Taberna, P. Simon, Y. Gogotsi, M. Salanne, *Nature materials* **11(4)** (2012) 306-310. https://doi.org/10.1038/nmat3260.

[3] C. Lekakou, O. Moudam, F. Markoulidis, T. Andrews, J.F. Watts, G.T. Reed, *Journal of Nanotechnology* **2011** (2011). https://doi.org/10.1155/2011/409382

[4] Y. Yang, Y. Han, W. Jiang, Y. Zhang, Y. Xu, A.M. Ahmed, *Applied Sciences* **12(1)** (2021) 354. https://doi.org/10.3390/app12010354

[5] H. Liu, C. Xu, Y. Ren, D. Tang, C. Zhang, F. Li, X. Wei, C. Huo, X. Li, R. Zhang, *ACS omega* **5(42)** (2020) 27032-27042. https://doi.org/10.1021/acsomega.0c02021

[6] S.J. Rajasekaran, V. Raghavan, *Diamond and Related Materials* **109** (2020) 108038. https://doi.org/10.1016/j.diamond.2020.108038

[7] P. Hong, X. Liu, X. Zhang, S. Peng, Z. Wang, Y. Yang, *International Journal of Energy Research* **44(2)** (2020) 988-999. https://doi.org/10.1002/er.4970

[8] Y. Zhang, S. Li, Z. Tang, Z. Song, J. Sun, *Diamond and Related Materials* **91** (2019) 119-126. https://doi.org/10.1016/j.diamond.2018.11.013

[9] C. Quan, *International Journal of Energy Research* **44(2)** (2020) 1218-1232. https://doi.org/10.1002/er.5017

[10] C. Quan, N. Gao, *International Journal of Energy Research* **44(6)** (2020) 4335-4351. https://doi.org/10.1002/er.5206

[11] S. Ahmed, M. Parvaz, R. Johari, & M. J. M. R. E Rafat, *Materials Research Express* **5(4)** (2018) 045601. http://dx.doi.org/10.1088/2053-1591/aab924

[12] E. Yi, L. Teo, L. Muniandy, E. Ng, F. Adam, A.R. Mohamed, R. Jose, K.F. Chong, *Electrochimica Acta* **192** (2016) 110-119. https://doi.org/10.1016/j.electacta.2016.01.140

[13] V. N. K. S. Kumar Nersu, B. R. Annepu, S. S. Babu Patcha, S. Singh Rajaputra, *Journal of Electrochemical Science and Engineering* **12(3)** (2022) 451-462. https://doi.org/10.5599/jese.1310

[14] J. Han, Y. Ping, J. Li, Z. Liu, B. Xiong, P. Fang, *Diamond and Related Materials* **96** (2019) 176-181. https://doi.org/10.1016/j.diamond.2019.05.014

[15] Y. Gao, Q. Yue, B. Gao, A. Li, *Science of the Total Environment* **746** (2020) 141094. https://doi.org/10.1016/j.scitotenv.2020.141094

[16] Z. Liu, Z. Zhu, J. Dai, Y. Yan, *Chemistry Select* **3(21)** (2018) 5726-5732. https://doi.org/10.1002/slct.201800609
[17] S.T. Neeli, H. Ramsurn, *Carbon* **134** (2018) 480-490. https://doi.org/10.1016/j.carbon.2018.03.079
[18] C. Bora, S.K. Dolui, *Polymer* **53(4)** (2012) 923-932. https://doi.org/10.1016/j.polymer.2011.12.054
[19] J. Zhang, S. Song, J. Xue, P. Li, Z. Gao, Y. Li, *International Journal of Electrochemical Science* **13** (2018) 5204-5218. http://dx.doi.org/10.20964/2018.06.09
[20] N. Mojoudi, N. Mirgha, M. Soleimani, H. Shariatmadari, C. Belver, J. Bedia, *Scientific Reports* **9(1)** (2019) 1-12. https://www.nature.com/articles/s41598-019-55794-4
[21] S. Nasir, M. Z Hussein, Z Zainal, N. A Yusof, & S. A Mohd Zobir, *Energies* **11(12)** (2018) 3410. https://doi.org/10.3390/en11123410
[22] T. Chen, N. Zhang, Z. Xu, X. Hu, Z. Ding, *Environmental Science and Pollution Research* **26(3)** (2019) 2523-2530. https://doi.org/10.1007/s11356-018-3789-x
[23] S. Kumar, R. Prakash, A. Alimuddin, J. Song, *Journal of Central South University of Technology* **17(6)** (2010) 1139-1143. https://doi.org/10.1007/s11771-010-0609-y
[24] A. Kumar, H.M. Jena, *Results in Physics* **6** (2016) 651-658. https://doi.org/10.1016/j.rinp.2016.09.012
[25] P. Bai, S. Wei, X. Lou, L. Xu, *RSC Advances* **9(54)** (2019) 31447-31459. https://doi.org/10.1039/C9RA06501F
[26] A.E. Ismanto, S. Wang, F.E. Soetaredjo, S. Ismadji, *Bioresource Technology* **101(10)** (2010) 3534-3540. https://doi.org/10.1016/j.biortech.2009.12.123
[27] A.N. Grace, R. Ramachandran, M. Vinoba, Y. Choi, *Electroanalysis* **26(1)** (2014) 199-208. https://doi.org/10.1002/elan.201300262
[28] A. Xu, Y Weng, & R Zhao, *Materials* **13(5)** (2020) 1179. https://doi.org/10.3390/ma13051179
[29] A. Bello, F. Barzegar, D. Momodu, *RSC Advances* **4(73)** (2014) 39066-39072. https://doi.org/10.1039/C4RA05425C
[30] C. Liu, W. Dong, G. Cao, J. Song, L. Liu, *Journal of the Electrochemical Society* **155(1)** (2007) F1. http://dx.doi.org/10.1149/1.2799683
[31] S. Sopčic, D. Antonić, Z. Mandić, K. Kvastek, V. Horvat-Radošević *Journal of Electrochemical Science and Engineering* **8(2)** (2018) 183-195. https://doi.org/10.5599/jese.536
[32] F. Bu, W. Zhou, Y. Xu, Y. Du, C. Guan, *Npj Flexible Electronics* **4(1)** (2020) 1-16. https://doi.org/10.1038/s41528-020-00093-6
[33] J. Jiang, L. Zhang, X. Wang, N. Holm, K. Rajagopalan, F. Chen, S. Ma, *Electrochimica Acta* **113** (2013) 481-489. https://doi.org/10.1016/j.electacta.2013.09.121
[34] S. Ahmed, A. Ahmed, M. Rafat, *Journal of Saudi Chemical Society* **22(8)** (2018) 993-1002. https://doi.org/10.1016/j.jscs.2018.03.002
[35] H. Aripin, L.A. Lestari, *The Open Materials Science Journal* **4(1)** (2010). http://dx.doi.org/10.2174/1874088X01004010117
[36] V. Subramanian, C. Luo, A.M. Stephan, K.S. Nahm, S. Thomas, *The Journal of Physical Chemistry C* **111(20)** (2007) 7527-7531. https://doi.org/10.1021/jp067009t
[37] M.R. Jisha, Y. Ju, J. Sun, K. Suk, T.P. Kumar, K. Karthikeyan, N. Dhanikaivelu, D. Kalpana, N.G. Renganathan, A.M. Stephan, *Materials Chemistry and Physics* **115(1)** (2009) 33-39. https://doi.org/10.1016/j.matchemphys.2008.11.010
[38] H. Chen, Y. Guo, F. Wang, G. Wang, P. Qi, X. Guo, B. Dai, *New Carbon Materials* **32(6)** (2017) 592-599. https://doi.org/10.1016/S1872-5805(17)60140-9
[39] M. Zhi, F. Yang, F. Meng, M. Li, A. Manivannan, N. Wu, *ACS Sustainable Chemistry & Engineering* **2(7)** (2014) 1592-1598. https://doi.org/10.1021/sc500336h